Razzaq, M.Y.; Behl, M.; Lendlein, A.:
Magneto-Mechanical Actuators with Reversible Stretching and Torsional Actuation Capabilities.
In: MRS Advances. Vol. 4 (2019) 19, 1057 - 1065.
First published online by Cambridge University Press: February 13, 2019

DOI: 10.1557/adv.2019.123
https://dx.doi.org/10.1557/adv.2019.123

Magneto-Mechanical Actuators with Reversible Stretching and Torsional Actuation Capabilities

M. Yasar Razzaq[a], M. Behl[a], A. Lendlein[a,b]

[a]*Institute of Biomaterial Science, Helmholtz-Zentrum Geesthacht, Kantstr. 55, 14513 Teltow, Germany*
[b]*Institute of Chemistry, University of Potsdam, 14476 Potsdam, Germany*

ABSTRACT

Composite actuators consisting of magnetic nanoparticles dispersed in a crystallizable multiphase polymer system can be remotely controlled by alternating magnetic fields (AMF). These actuators contain spatially segregated crystalline domains with chemically different compositions. Here, the crystalline domain associated to low melting transition range is responsible for actuation while the crystalline domain associated to the higher melting transition range determines the geometry of the shape change. This paper reports magneto-mechanical actuators which are based on a single crystalline domain of oligo(ω-pentadecalactone) (OPDL) along with covalently integrated iron(III) oxide nanoparticles (ioNPs). Different geometrical modes of actuation such as a reversible change in length or twisting were implemented by a magneto-mechanical programming procedure. For an individual actuation mode, the degree of actuation could be tailored by variation of the magnetic field strengths. This material design can be easily extended to other composites containing other magnetic nanoparticles, e.g. with a high magnetic susceptibility.

INTRODUCTION

Magneto-mechanical actuators are relevant for artificial muscles and their applications for humanoid robots, smart fabrics and exoskeletons [1-12]. Alternating magnetic field (AMF) provides remote heating of magnetic particles in a nanocomposite by hysteresis or relaxational mechanisms [6, 7, 13-18]. This remote heating is useful to initiate the actuation of thermo-sensitive polymer nanocomposites e.g., smart hydrogels, ferrogels, liquid crystalline elastomers (LCE) [6, 19]. Remote controlled contraction/expansion of magnetic nanocomposites of poly(*n*-isopropylacrylamide) (PNIPAAm) for drug release and microfluidic applications has been reported [20]. Incorporation of iron(III) oxide nanoparticles (iONP) in LCE enabled a reversible change in length which was remotely controlled by AMF [1]. Recently, magnetic actuators based on crystallizable polymer nanocomposites with chemically heterogeneous structure were reported [14]. The nanocomposite consisted of two separate crystallizable structural units with distinct melting (T_m) and crystallization temperatures (T_c) along with covalently integrated ioNPs. Thermo-mechanical programming of these nanocomposites resulted in an oriented actuating domain (AD) (with lower T_m), which maintained its orientation, while undergoing thermal transition by exposure to AMF. Cooling of the composite by switching off the AMF, lead to a directed crystallization of the AD enabling a macroscopic

shape change process. Reheating by exposure to AMF caused the melting of the crystalline domains and an entropy-driven contraction of the sample [21]. However, the heterogeneous morphology of these nanocomposites significantly affected the distribution of the ioNPs and the actuation capability. We hypothesized that magnetic nanocomposites with a homogenous structure based on one chemical component would enable a uniform distribution of ioNP and a higher actuation capability by mean of AMF inputs.

Our concept to synthesize magnetic nanocomposites with a homogenous structure is to use one crystallizable oligomer with the same type of repeating unit. Here, the covalent integration of ioNP can be used to improve the distribution of the nanoparticles into the matrix. However, the challenge is the adjustment of actuating and geometry stabilizing domain by magnetic heating. Nevertheless, these type of hybrid nanocomposites with covalently integrated ioNP have shown a thermal actuation by exposure to environmental heating [22]. The covalent integration of ioNP resulted in a uniform distribution and an improved elastic modulus at higher temperatures [13].

Our strategy to realize such an actuation in a composite material with single crystalline unit was to use one fraction of aligned crystals to fix the programmed shape, whereas the other fraction could be utilized to provide reversible actuation when the AMF is switched on-off. The AMF would enable a precise heating of the nanocomposite to achieve the temperatures in the melting range of the crystalline domain. The memory of the original shape could be erased by the use of a higher magnetic field strength to melt all the crystals and to enable the reprogramming to a new desired shape.

Oligo(ω-pentadecalactone) (OPDL) based magnetic nanocomposites (OPDL-NC) with covalently anchored ioNPs were selected for the design of the composite materials with actuating unit from one component. Compared to oligo(ε-caprolactone), OPDL enables high transition temperature and fast crystallization and could be a suitable selection for magnetically triggered actuators [23]. The synthesis of OPDL-NC was carried out according to the methods reported in [24, 25]. In exploratory experiments it was found that 5 wt % of ioNP content was capable to overcome the melting enthalpy of the OPDL crystalline domain during heating when exposed to an AMF with a f = 254 kHz [13]. The thermal analysis of the OPDL-NC enabled a glass transition temperature (T_g) at -70 °C and T_m = 74 °C with a melting range (ΔT_m) from 38 °C to 80 °C [22]. Microscopic analysis of these nanocomposites resulted in a uniform distribution of ioNP without any particle sedimentation [25]. The Young's modulus of the composite increased from 2.8 MPa for pure OPDL network to 3.5 MPa for OPDL-NC with 5 wt% of ioNPs at 90 °C. Similarly, a slight increase in the tensile strength from 1.0 MPa for pure OPDL network to 1.5 MPa for the OPDL-NC at 90 °C was observed [25]. Here, different magnetic field strengths were used to partially melt the crystalline domain and achieve the tailorable actuation in different modes, e.g. elongation/contraction and twisting. The partial melting of the OPDL crystalline domain by application of different magnetic field strengths is schematically demonstrated in Figure 1.

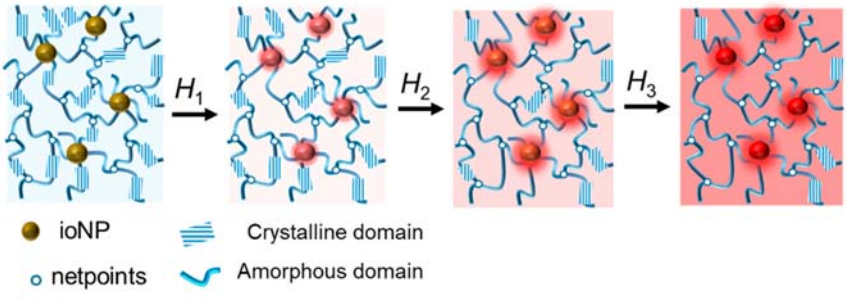

Figure 1: Schematic representation of the molecular mechanism of the tailorable actuation of the OPDL-NC by exposure to different magnetic field strengths.

EXPERIMENTAL DETAILS

Inductive heating was accomplished by positioning the sample in an alternating magnetic field at a frequency of f = 258 kHz. The equipment consisted of a high-frequency generator (TIG 5/300; Huettinger Electronic, Freiburg, Germany) and a water-cooled copper coil (6 loops, diameter 4 cm, height 4.5 cm). The magnetic field strength H could be adjusted by variation of the power output of the generator.

The magneto-mechanical experiments were conducted with a Zwick Z2.5 (Ulm, Germany) tensile tester, which was combined with the high frequency generator. The samples were fixed with plastic clamps in the center of the inductor. The programming by stretching under the effect of magnetic field was controlled by the tensile tester, the magnetic field strength was manually controlled by adjusting the power output of the generator.

Cyclic, magneto-mechanical experiments were carried out by exposing the nanocomposite (25 × 5 × 1 mm^3) to H_{high} = 18 $kA \cdot m^{-1}$ and stretching to ε_{def} = 40% with a strain rate of 5 $mm \cdot min^{-1}$. After equilibration for 5 min, the magnetic field strength was switched to H_{low} = 0 $kA \cdot m^{-1}$ and the stress was lowered to 20 mN. Increase of the magnetic field strength from H_{low} to H_1 = 11 $kA \cdot m^{-1}$, H_2 = 11.5 $kA \cdot m^{-1}$ or H_3 = 12 $kA \cdot m^{-1}$ with a rate of 0.2 $kA \cdot m^{-1} \cdot min^{-1}$, resulted in the recovery of the sample to ε_A. The magnetic field was lowered to H_{low} = 0 $kA \cdot m^{-1}$ with a rate of 0.2 $kA \cdot m^{-1} \cdot min^{-1}$and the length of the sample was increased to ε_B. When the magnetic field strength was increased to H_1, H_2 or H_3, the length of the sample decreased back to ε_A. The cyclic change of the magnetic field strength between H_{low} and higher magnetic field strengths (H_1, H_2 or H_3) was repeated for three cycles.

The cyclic, magneto-mechanical experiments for monitoring the contractual stress (σ_{contr}) during actuation cycles, were carried out by deforming the sample to ε_{def} = 40% at H_{high} = 18 $kA \cdot m^{-1}$ with a strain rate of 5 $mm \cdot min^{-1}$ and then subsequently equilibrating for 5 min. The sample was then cooled to room temperature by switching the magnetic field strength to H_{low} under strain controlled conditions. After 5 min waiting time, the sample was unloaded to a stress value of σ = 20 mN. Application of H_1, H_2 or H_3 for 5 min resulted in the recovery of the sample to ε_A. When the magnetic field was switched off (H_{low}) for 5 minutes, the length of the sample was increased to ε_B. Here, the strain was kept constant and exposure to H_1, H_2 or H_3 was carried out, during which σ_{contr} was recorded. The sample was again cooled by application of H_{low} followed by a waiting period

of 5 min. The exposure to magnetic field and cooling by application of H_{low} were repeated three times.

The cyclic, twisting experiments were carried out by connecting the top end of the nanocomposite film (25 × 5 × 1 mm^3) to a rotatable plastic clamp and the bottom end to a fixed clamp while being kept in the center of the magnetic coil. During twisting, the magnetic field strength was kept constant at H_{high} = 18 kA·m^{-1} and the nanocomposite film was rotated to θ_{rot} = 360° and the magnetic field strength was switched to H_{low}. Subsequently, the bottom end of the actuator was detached from the clamp to enable a free-standing reversible uncoiling/coiling. The reversible rotation of the composite film was recorded by a video camera (Canon HFG10), and the angles were measured from snapshots by software Image J (National Institutes of Health, Bethesda, USA).

RESULTS AND DISCUSSIONS

In a preliminary experiment, the magnetic heating capability of the nanocomposite film was examined by exposing it to an AMF of a fixed frequency (f = 254 kHz). Different magnetic field strengths H_1 = 11 kA·m^{-1}, H_2 = 11.5 kA·m^{-1}, H_3 = 12 kA·m^{-1} enabled the temperatures T_{H1} = 60 ±1 °C, T_{H2} = 64 ±1 °C and T_{H3} = 70 ±1 °C (Figure 2a). Further increase of the magnetic field strength to H_{high} = 18 kA·m^{-1}, resulted in the complete melting of the OPDL crystalline domains when the temperature T_{high} = 85 ±1 °C was achieved (Figure 2b).

To investigate the tailored actuation capability, the nanocomposite was programmed by exposing the film to H_{high} and stretching to ε_{def} = 40% of its original length. The lower stretching ratio was used to minimize the effects of changes in temperature during stretching as the sample temperature is a function of its surface area. Afterwards, the magnetic field strength was switched off to fix the alignment of the polymer chain segments by their solidification and the stress was removed. Increase of the magnetic field strength from H_{low} = 0 kA·m^{-1} to H_1 = 11 kA·m^{-1} resulted in the melting of a small fraction of AD, which causes the partial recovery of the sample to the ε_A = 32%.

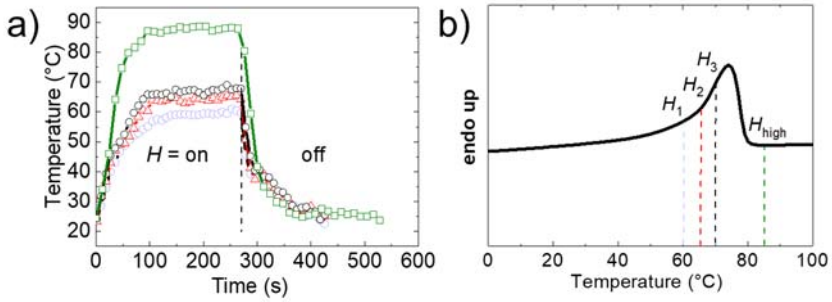

Figure 2: a) Temperature profiles of the OPDL-NC achieved by exposure to different field strength H: H_1 = 11.0 kA·m^{-1} (blue hexagons); H_2 = 11.5 kA·m^{-1} (red triangles); H_3 = 12.0 kA·m^{-1} (black circles); H_{high} = 18 kA·m^{-1} (green squares). b) DSC thermogram of the OPDL-NC indicating the temperatures achieved by exposure to different magnetic field strengths in the melting range of the OPDL crystalline domain.

When the magnetic field was lowered to H_{low}, the heating of the anchored ioNP stopped and the oriented recrystallization of the chain segments resulted in a slight increase in the length of the sample to $\varepsilon_B = 34\%$. The increase in the length of the sample could be reversed to ε_A by increasing the magnetic field strength to H_1 enabling a melting induced contraction (MIC) of the composite. The reversible change in the length of the sample was repeated ($n = 3$) by cyclic change of the magnetic field strength between H_1 and H_{low} under stress free conditions resulting in reversible actuation of $\varepsilon_{rev} = 1.8 \pm 0.1\%$. To tailor the actuation performance, the applied magnetic field strength was increased to H_2 during recovery of the programmed sample. The application of H_2 caused the melting of a larger crystalline fraction of AD thus enabling the recovery of the composite to $\varepsilon_A = 25\%$. The cyclic change of the magnetic field strength between H_{low} and H_2 resulted in a higher ε_{rev} of $4.5 \pm 0.2\%$ which is attributed to the increased quantity of the crystalline AD. Increasing the magnetic field strength to H_3 increased the recoverable strain to $\varepsilon_A = 11\%$, which was reversibly switched between ε_A and $\varepsilon_B = 18\%$, enabling a maximum value of ε_{rev} of $6 \pm 0.2\%$. The cyclic change in the length of the composite for the third cycle by application of three different magnetic field strengths is shown in Figure 3a and the values of ε_{rev} at different magnetic field strengths are provided in Table 1. The increase in the value of ε_{rev} by increasing the applied magnetic field strength is attributed to the increased quantity of crystals involved in actuation. Here, it has to be clarified that the further increase of the magnetic field strength caused the complete melting of the crystalline domain enabling the recovery to its original state and a loss of the reversible actuation. Here, the geometry stabilizing fraction of crystals will be melted and the entropy driven recovery to the original length will take place. The previously reported multiphase nanocomposite could enable an actuation of $\varepsilon_{rev} = 3 \pm 0.2\%$ in the stretching mode. Here, the low actuation capability was attributed to the structurally heterogeneous polymer system and nonhomogeneous distribution of the ioNPs [14].

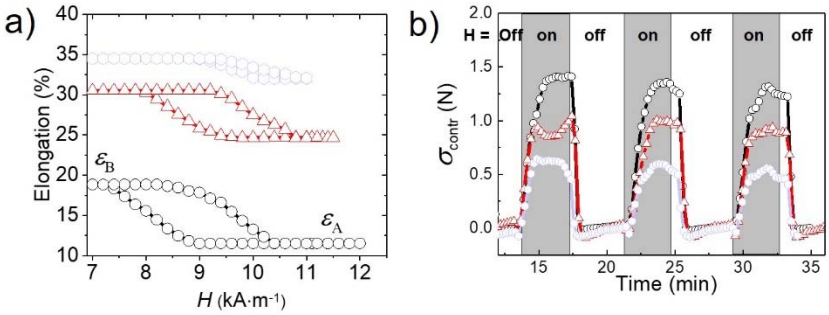

Figure 3: a) Reversible change in the length of the composite by application of different magnetic field strengths, $H_3 = 12$ kA·m^{-1} (black circles), $H_2 = 11.5$ kA·m^{-1} (red triangles), $H_1 = 11$ kA·m^{-1} (grey hexagons). b) Recovery stress during tailorable actuation of the composite by application of different magnetic field strengths, $H_3 = 12$ kA·m^{-1} (black circles), $H_2 = 11.5$ kA·m^{-1} (red triangles), $H_1 = 11$ kA·m^{-1} (blue hexagons).

Table 1: Reversible change in elongation, contractual stress and twisting angle of the OPDL-NC by application of different magnetic field strengths.

H (kA·m^{-1})[a]	ε_{rev} (%)[b]	σ_{contr} (N)[c]	$\Delta\theta$ (°)[d]
11.0	1.8 ± 0.1	0.60 ± 0.04 N	31 ± 1
11.5	4.5 ± 0.2	0.91 ± 0.03 N	43 ± 1
12.0	6.0 ± 0.2	1.40 ± 0.10 N	70 ± 1

[a] Magnetic field strength applied during actuation [b] Reversible change in the length of the composite [c] Contractual stress of the composite during actuation [d] Change in the twisting angle during torsional actuation.

Similar to the increased actuation capability, the contractual stress (σ_{contr}) of the NC-OPDL (measured under strain controlled conditions) was also increased by increasing the magnetic field strength. When the programmed sample was exposed to the magnetic field, it contracted because of the partial melting of the crystalline domains and σ_{rec} reached a maximum (Figure 3b). When the magnetic field was switched off to H_{low}, σ_{contr} began to dissipate and reached to 0 N within a short interval of time (40 s). The value of σ_{contr} was increased from 0.6 ± 0.04 N for H_1 to 1.4 ± 0.10 N achieved by application of H_3 (Table 1). The increase in σ_{contr} by increasing magnetic field strength is attributed to the melting of the higher fraction of the AD.

The actuation mode of the OPDL-NC from reversible elongation could be changed by reprogramming the composite by application of H_{high}, which enabled the complete melting of the OPDL crystalline domain. The nanocomposite film could also act as a torsional actuator; while the sample was exposed to H_{high}, it was twisted. The composite film was programmed by twisting to an angle of 360° (~ 1 turn). A schematic demonstration of the torsional actuation is shown in Figure 4a. A higher number of turns resulted in breakage of the composite film. The application of three different magnetic field strength H_1, H_2, and H_3 resulted in a tailorable torsional actuation profile as shown in Figure 4b. An exposure to H_1, enabled an uncoiling of the actuator from 0° to 31°. The actuator could be coiled back to an original angle of 0° by switching the magnetic field to H_{low}. By increasing the magnetic field strength to the value of H_2, the reversible change in the twisting angle was increased to 43±1°. When the applied magnetic field strength was further increased to H_3, the melting of the highest possible volume fraction of the crystalline domains occurred and caused an reversible angle change of $\Delta\theta$ = 70±1° (Table 1). The image series in Figure 4c exemplarily shows the reversible change in the twisting angle when the actuator was exposed to a magnetic field strength H_3.

Compared to the thermal actuation by changing the environmental temperature [22], the magnetic actuation by exposure to AMF is a faster process, as maximized heating/cooling rates (~ 40 K·min^{-1}) are obtained by either switching the magnetic field *on* or *off* [26]. However, a slightly higher ε_{rev} = 8.2 ± 0.2% of the hybrid composite with same ioNP content was obtained by environmental heating and can be attributed to the higher ε_{def} applied in thermochamber [22].

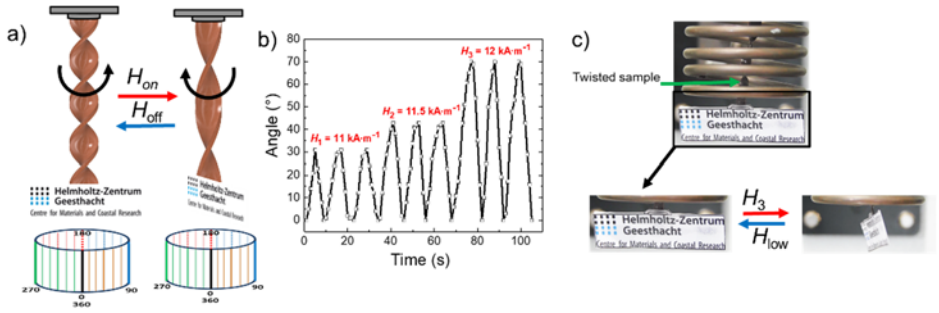

Figure 4. a) Schematic demonstration of the torsional actuation of the composite by switching the AMF on and off. To visualize the twisting angle, logo of Helmholtz-Zentrum Geesthacht is attached below. b) Changes of the twisting angle (θ) by switching between H_{low} and H_1 = 11 kA·m^{-1} or H_2 = 11.5 kA·m^{-1} or H_3 = 12 kA·m^{-1}, during three cycles. c) Figure series exemplarily showing the reversible change in the twisting angle when exposed to a cyclic change of magnetic field strength between H_{low} and H_3.

The microstructural changes during actuation process were monitored by two dimensional wide-angle X-ray scattering (2D-WAXS). In these experiments, the nanocomposite film was programmed (ε_{def} = 40%) and was partially recovered by application of H_1, H_2 or H_3. Switching the magnetic field strength to H_{low} resulted in an elongation to ε_b. Afterwards, the sample was removed from the inductor coil, and placed into the WAXS sample holder. The original, non-deformed sample, showed two sharp reflections of (110) and (200) planes at room temperature, which appear at the peak positions of about 2θ = 21.4° and 23.8° corresponding to d = 1.17 and 3.73 Å, respectively with a degree of crystallinity (DOC) of 25 ± 0.2% [25]. The diffraction pattern of the original and programmed sample which has undergone an oriented crystallization is shown in Figure 5a(i, ii) (exemplarily shown for sample programmed by application of H_3). The orientation of the AF resulted a brighter (110) reflection and a slight increase in the DOC = 30 ± 1% of the composite, which can be attributed to strain induced crystallization of the polymer chains [13]. The azimuthal profiles (I vs χ) of the (110)-reflection of crystalline OPDL in the composite programmed at H_3 are depicted in Figure 5b. The intensity of the profile is related to the degree of orientation of the (110)-symmetry plane and thus to the crystal orientation in the specimen. The intensified (110) peak showed a bimodal behavior as the reflection was split into two peaks, which was attributed to the tilted orientation of the crystals caused by ioNPs acting as crosslinks. The oriented crystallization of the actuating fraction was melted by increasing the environmental temperature to T_{H3} = 70±1 °C, which is equivalent to the temperature achieved during inductive heating by exposure to H_3. After heating, the actuating crystals were melted, resulting in a decrease in the intensities of the 110 and 200 reflections. The heating caused a decrease in the DOC of the nanocomposite to 19 ± 1% (Figure 5a, iii and 5b) and was attributed to the melting of the actuating part of the crystalline domain. By cooling the sample again to ambient temperature, the DOC was restored to the original value of 30 ± 1%.

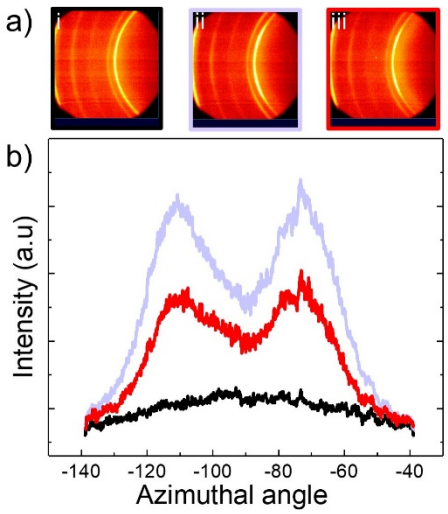

Figure 5: a) WAXS pattern of the (i) original nanocomposite sample (ii) 3rd actuation cycle; while cooled at H_{low} (iii) heated to T_{H3}. For coloured image, please see online version. b) Azimuthal plot with radial angle χ vs Intensity (I) of (110) equatorial reflection (in arbitrary units), original un-programmed sample (black), 3rd actuation cycle; while cooled at H_{low} (blue/light grey) heated to T_{H3} (red/dark grey).

The similar changes in the DOC were also observed when the programmed samples were heated to T_{H2} and T_{H1}. Summarizing the WAXS investigations, it can be said that the reversible actuation is a result of a directed crystallization of the actuating fraction forming lamellae in the direction assigned by the crystals acting as stabilizing fraction, when the nanocomposite cools at H_{low}, whereby the actuation is reversed upon melting by exposure to variable magnetic field strengths.

CONCLUSION

In conclusion, the synthesis of a magnetic nanocomposite with covalently integrated ioNPs in OPDL based matrix facilitated magneto-mechanical actuators with reversible stretching and torsional actuation capabilities. The higher actuation capability ($\varepsilon_{rev} \sim 6 \pm 0.2\%$) of the hybrid composite compared to the previously reported multiphase actuators was attributed to the homogenous structure of the nanocomposite and uniformly distributed nanoparticles. Here, the OPDL crystalline domain was divided into an actuating and geometry stabilizing fraction enabling a tailorable actuation by application of variable magnetic field strengths. Furthermore, the actuation mode of the composite film could be switched from stretching to torsional modes depending on the requirement. Magneto-mechanical actuations in stretching mode resulted in a reversible change in length of the sample enabling ε_{rev} values ranging from $1.8 \pm 0.1\%$ to $6 \pm 0.2\%$. In torsion mode the twisting angle could be adjusted from $31 \pm 1°$ to $70 \pm 1°$. The increase in the actuation performance in different modes was attributed to the increasing fraction of crystals acting as actuating domain. These magneto-mechanical actuators are relevant for remote controlled sensors and switches.

ACKNOWLEDGMENTS

The authors gratefully thank the Helmholtz Association for funding of this work through program-oriented funding.

References

1. A. Garcia-Marquez, A. Demortiere, B. Heinrich, D. Guillon, S. Begin-Colin and B. Donnio, J Mater Chem 21, 8994 (2011).
2. J.M. Park, S.J. Kim, J.H. Jang, Z.J. Wang, P.G. Kim, D.J. Yoon, J. Kim, G. Hansen and K.L. DeVries, Compos Part B-Eng 39, 1161 (2008).
3. M.M. Said, J. Yunas, B. Bais, A.A. Hamzah and B.Y. Majlis, Micromachines-Basel 9 (2018).
4. R. Fuhrer, E.K. Athanassiou, N.A. Luechinger and W.J. Stark, Small 5, 383 (2009).
5. M.M. Said, J. Yunas, R.E. Pawinanto, B.Y. Majlis and B. Bais, Sensor Actuat A-Phys 245, 85 (2016).
6. J. Thevenot, H. Oliveira, O. Sandre and S. Lecommandoux, Chem Soc Rev 42, 7099 (2013).
7. R.T. Woodward, C.I. Olariu, E.A. Hasan, H.H.P. Yiu, M.J. Rosseinsky and J.V.M. Weaver, Soft Matter 7, 4335 (2011).
8. L.K. Lagorce, O. Brand and M.G. Allen, J Microelectromech S 8, 2 (1999).
9. D. Szabo, G. Szeghy and M. Zrinyi, Macromolecules 31, 6541 (1998).
10. H. Lee, J. Kim, J. Kim, S.E. Chung, S.-E. Choi and S. Kwon, Nat Mater 10, 747 (2011).
11. M. Zrinyi, Colloid Polym Sci 278, 98 (2000).
12. V.Q. Nguyen, A.S. Ahmed and R.V. Ramanujan, Adv Mater 24, 4041 (2012).
13. M.Y. Razzaq, M. Behl, K. Kratz and A. Lendlein, Adv Mater 25, 5730 (2013).
14. L. Wang, M.Y. Razzaq, T. Rudolph, M. Heuchel, U. Nochel, U. Mansfeld, Y. Jiang, O.E.C. Gould, M. Behl, K. Kratz and A. Lendlein, Mater Horiz 5, 861 (2018).
15. S. Campbell, D. Maitland and T. Hoare, ACS Macro Lett 4, 312 (2015).
16. X.L. Liu, G. Zhao, Z.R. Chen, F. Panhwar and X.M. He, ACS Appl Mater Inter 10, 16822 (2018).
17. F.H. Zhang, Z.C. Zhang, C.J. Luo, I.T. Lin, Y.J. Liu, J.S. Leng and S.K. Smoukov, J Mater Chem C 3, 11290 (2015).
18. H. Meng and J. Hu, J Intel Mat Syst Str 21, 859 (2010).
19. M. Ma, Y. Zhang, X.L. Shen, J. Xie, Y. Li and N. Gu, Nano Res 8, 600 (2015).
20. Y.H. Lien, T.M. Wu, J.H. Wu and J.W. Liao, J Nanopart Res 13, 5065 (2011).
21. M. Behl, K. Kratz, J. Zotzmann, U. Nochel and A. Lendlein, Adv Mater 25, 4466 (2013).
22. M.Y. Razzaq, M. Behl and A. Lendlein, MRS Advances, doi:10.1557/adv.2018.613 (2018).
23. A. Arnebold and A. Hartwig, Polymer 83, 40 (2016).
24. M.Y. Razzaq, M. Behl, U. Frank, J. Koetz, W. Szczerba and A. Lendlein, J Mater Chem 22, 9237 (2012).
25. M.Y. Razzaq, M. Behl, U. Nochel and A. Lendlein, Polymer 55, 5953 (2014).
26. M.Y. Razzaq, M. Behl and A. Lendlein, MRS Soc Symp Proc 1718, 71 (2015).